

ON THE FERMI GBM EVENT 0.4 SEC AFTER GW 150914

J. GREINER^{1,2}, J.M. BURGESS^{3,4}, V. SAVCHENKO⁵, H.-F. YU^{1,2}

¹Max Planck Institute for Extraterrestrial Physics, Giessenbachstrasse, 85748 Garching, Germany

²Excellence Cluster Universe, Technische Universität München, Boltzmannstraße 2, 85748, Garching, Germany

³Oskar Klein Centre for Cosmoparticle Physics, SE-106 91 Stockholm, Sweden

⁴Dept. of Physics, KTH Royal Institute of Technology, AlbaNova, SE-106 91 Stockholm, Sweden

⁵Francois Arago Centre, APC, Université Paris Diderot, CNRS/IN2P3, CEA/Irfu, Observatoire Paris, Sorbonne Paris Cité, 10 rue Alice Domon et Léonie Duquet, 75205 Paris Cedex 13, France

ABSTRACT

In view of the recent report by [Connaughton et al. \(2016\)](#) we analyse continuous TTE data of Fermi-GBM around the time of the gravitational wave event GW 150914. We find that after proper accounting for low count statistics, the GBM transient event at 0.4 s after GW 150914 is likely not due to an astrophysical source, but consistent with a background fluctuation, removing the tension between the INTEGRAL/ACS non-detection and GBM. Additionally, reanalysis of other short GRBs shows that without proper statistical modeling the fluence of faint events is over-predicted, as verified for some joint GBM-ACS detections of short GRBs. We detail the statistical procedure to correct these biases. As a result, faint short GRBs, verified by ACS detections, with significances in the broad-band light curve even smaller than that of the GBM-GW150914 event are recovered as proper non-zero source, while the GBM-GW150914 event is consistent with zero fluence.

Keywords: gamma-rays: general — gravitational waves — methods: statistical

1. INTRODUCTION

The gravitational wave (GW) era started with an overwhelmingly strong and convincing event (called GW 150914), reported to originate from an unexpected source of a massive black hole binary merger ([Abbott et al. 2016](#)). Neither were merger rates of such massive binaries well established (but see [Belczynski et al. 2010](#), for optimistic rates), nor is it clear whether or not one should expect an electromagnetic signal ([Perna et al. 2016](#); [Lyutikov 2016](#)). Finding the electromagnetic counterpart is the next challenge which is difficult also because of the large error circles of the present GW detection capability ([Abbott et al. 2016](#)).

With the all-sky gamma-ray burst monitor (GBM) onboard the Fermi satellite a flaring event with a signal-to-noise ratio of 5.1 and a false alarm probability of 0.2–2.8% (depending on the assumed likelihood distribution over the search window) was reported ([Connaughton et al. 2016](#)). If true, and indeed related to the GW event, this would be a fascinating discovery, allowing truly astrophysical constraints on the massive black hole binary merger. In view of this importance of correlated electromagnetic signals to gravitational wave events, particular scrutiny is required in the evaluation of candidate electromagnetic signals. Here, we report some additional analysis of the Fermi/GBM data.

We approach our analysis in two steps. First, we examine methodology implemented in the standard GBM analysis tools and improve upon it paying special attention to the statistical nature of the data in light of the fact that the alleged source is weak and background dominated (Fig. 1, Sect. 2). Next, we repeat the spectral analysis following the approach of [Connaughton et al. \(2016\)](#) using the standard tools for GBM analysis as well as examine the surrounding temporal background spectrum (Sect. 3). Finally, we implement a more statistically advanced approach to the spectral analysis which leads us to the conclusion that the source spectrum is more consistent with the background, rather than a short-hard GRB (Sect. 4). After demonstrating consistency with the INTEGRAL/ACS non-detection (Sect. 5), we conclude that caution should be taken with interpreting the GBM event as an astrophysical source.

2. GBM DATA ANALYSIS

The GBM is a non-imaging instrument relying on temporal isolation of signal against background. In practice, an observer identifies a source time interval in the light curve by its transient nature, compared to the smoothly-varying behavior of the background. Sophisticated algorithms may be applied to identify this source time interval,

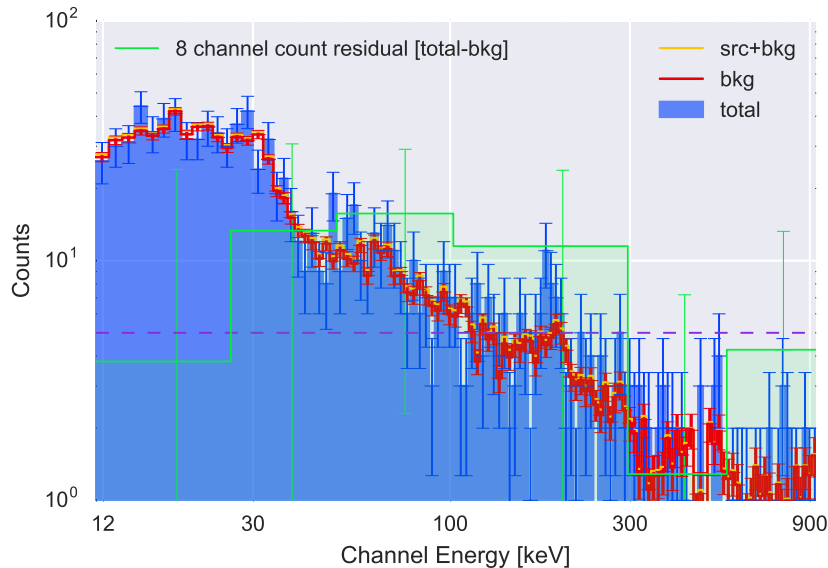


Figure 1. Spectral distribution of counts for the GBM event between 0.384-1.402 s in NaI 5. Shown are the total raw counts (blue), the background model from our fitted polynomial (red), the background plus source model (yellow) using the spectral parameters from our fit, and the residual source counts (green) rebinned into exactly the 8-channel spectrum as used in [Connaughton et al. \(2016\)](#), with the lowest (4-8 keV) and highest (overflow, i.e. >1 MeV) channel omitted. The highest-count channel is the one at 50–100 keV with 13 counts, demonstrating the low-count regime of the spectrum. The purple dashed line indicates the level at which the χ^2 background fitting method breaks down. The blue and green error bars show the [Skellam \(1946\)](#) confidence intervals.

i.e., Bayesian blocks ([Scargle et al. 2013](#)), signal-to-noise threshold, etc. Regardless, once a source time interval is identified, the background must be modeled so that it can be properly accounted for in spectral fitting of the source interval. Therefore, GBM spectral analysis consists of a two-step process, temporal fitting of the background lightcurve and subsequent fitting of the source spectra. We will detail both processes in the following two sub-sections.

As a starting note, we recall that the event reported by [Connaughton et al. \(2016\)](#) was not identified by any of the standard undirected offline GBM search procedures, due to its faintness. Instead, it was identified by a targeted search, seeded with the time of the GW event ([Blackburn et al. 2015](#)). Indeed, the count distribution of the event is fully consistent with the noise distribution before and after the event. Two numbers given in [Connaughton et al. \(2016\)](#) are particularly worth noting:

(i) One is the signal-to-noise ratio $\text{SNR} = 5.1$ (corresponding to a significance of $\lesssim 3\sigma$) as given in their Fig. 2. This estimate is not determined purely on raw counts, but uses a spectral model (chosen to be a Band function with a low-energy power law of spectral slope 0 for the energy range where most counts are detected) to create, for a given sky location, a model rate per energy channel which then is used to weight the raw counts of the different detectors for the summing towards a “signal-to-noise optimized light curve” ([Connaughton et al. 2016](#)). While this hard spectral model best matched the observed counts in the GBM detectors ([Connaughton et al. 2016](#)), we show below that a more appropriate spectrum has a spectral index of -1.8 , thus lowering the SNR.

(ii) The other important number is the false alarm probability of 0.2% ([Connaughton et al. 2016](#)) which corresponds to 2.9σ , which is calculated from the measured false alarm rate of spectrally hard events in 2.5 days of GBM data, while that of spectrally soft events is larger (see Fig. 3 in [Connaughton et al. \(2016\)](#)). Due to this reason, the given false alarm probability of 0.2% is an optimistic lower limit.

2.1. Background Behaviour

Due to the nature of GBM backgrounds, it is difficult to define a spectral background model. The background contains a superposition of astrophysical, terrestrial, solar, and instrumental sources, each with its own time variability. Therefore, an assumption is made that in each GBM energy channel, the background is smoothly varying with time. With this assumption one selects a time interval before and after the source time interval and fits a polynomial in time to the count evolution to these time intervals but excluding the source time interval. This polynomial is then interpolated through the source time interval to estimate the background counts in each energy channel during the time of source activity. A major assumption of this approach is that the background does not vary during the source time interval more than the smooth nature apparent in the surrounding background time interval. This assumption is most likely valid if the source time interval is short compared to the time scale of the variations of the fitting polynomial.

To determine the polynomial shape of the temporal background count evolution, a fit to statistically fluctuating data

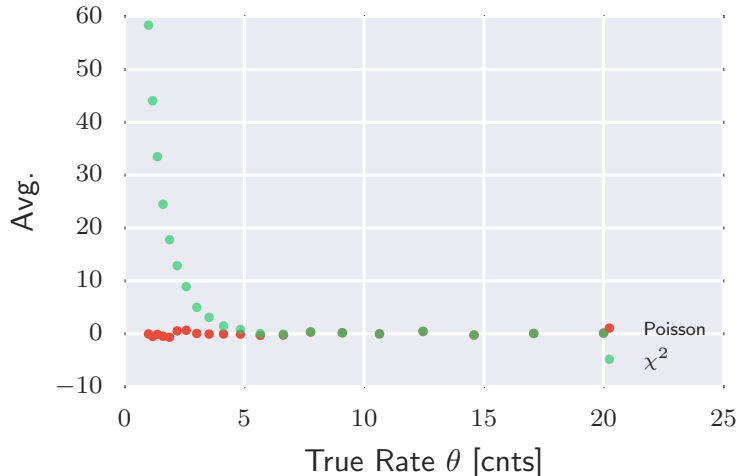


Figure 2. The average percent difference between the simulated and recovered θ as a function of the true rate for both the Poisson and χ^2 background fitting methods. While the modification of χ^2 made in RMFIT (weighted χ^2) improves the results, it still a poor statistic at very low-counts which frequently occur in high-energy channels.

must be performed. Under the assumption that these counts should be Poisson distributed, the statistic to choose for maximum-likelihood estimation (MLE) is the Poisson likelihood (e.g. the so-called Cash statistic, [Cash 1979](#)):

$$L = \prod_{i=1}^N \frac{M_i^{S_i} e^{-M_i}}{S_i!} \quad (1)$$

where M_i and S_i are the model and detected counts in the i^{th} of N bins, respectively. Taking the $-2 \log L$ and approximating the factorial term with Stirling's approximation ([Abramowitz & Stegun 2002](#))*, we have:

$$-2 \log L \approx 2 \sum_{i=1}^N M_i - S_i \log M_i + S_i \log S_i - S_i \quad (2)$$

$$= 2 \sum_{i=1}^N M_i - S_i + S_i (\log S_i - \log M_i). \quad (3)$$

The polynomial coefficients can be estimated via minimizing the log-likelihood of the background data and the polynomial integrated over each time bin.

In the RMFIT[†] software, generally used for GBM GRB data, the approach for determining the background is similar to the above method, except a weighted least-squares (χ^2) statistic is chosen to fit the polynomial coefficients via a two-pass method. First, the polynomial coefficients are estimated by solving the least-squares linear equations assuming that the data variance is equal to the number of counts. Then, the fit is performed again, but using the variance of the model determined in the first pass. This is intended to compensate for the fact that at low counts, the Gaussian approximation of the Poisson distribution is poor.

In the high-count regime, this approach may be valid. However, due to the fact that a polynomial is fit in each energy channel and that the background has fewer counts at high energies, the χ^2 statistic can be very biased ([Baker & Cousins 1984](#); [Humphrey et al. 2009](#); [Andrae et al. 2010](#)). To estimate this effect, we simulate synthetic light curves obeying a zero-order polynomial evolution in time over a period of 20 seconds. We choose a set of levels for the background mean rate (θ) ranging from 1-100 cts s⁻¹. For each θ , we simulate 500 lightcurves, and fit a polynomial to them with two different statistics criteria: Cash, and χ^2 . We find that the Cash statistic well recovers the true θ even at very low counts, while both χ^2 methods have a large bias at low counts (see Fig. 2). Therefore, we will use the Poisson likelihood to fit the background in our spectral analysis, but will compare the results to what is found using RMFIT and χ^2 .

* We note that this final form is sometimes referred to as the Castor statistic. However, it is simply the full Poisson likelihood, and its likelihood ratio asymptotically approaches a χ^2 distribution under the condition that the Fisher information matrix is positive definite, i.e., the model is linear in its parameters ([Wilks 1938](#)). Often, the terms dependent only on the data are dropped as they do not affect minimization ([Cash 1979](#)).

[†] <http://fermi.gsfc.nasa.gov/ssc/data/analysis/rmfit/>

2.2. Spectral Fitting Statistics

In the low source count regime, the choice of spectral fitting statistic is crucial. The total count rate in a source interval is distributed as a Poisson process, but we have more information via the background fit to better constrain the spectral fit parameters. The total counts in a spectral bin (S_i), is composed of source and background (B_i). Since we have estimated the background via a polynomial model, we can include this information in the Poisson likelihood. Let $P(t; \vec{\theta})$ be the estimated polynomial background rate model in a given energy channel where t is time and $\vec{\theta}$ are the polynomial coefficients. Then, for a given source interval from time T_1 to T_2 , we have

$$B_i = \int_{T_1}^{T_2} P(t; \vec{\theta}) dt. \quad (4)$$

Now, $\vec{\theta}$ are fitted coefficients with associated statistical errors and therefore B_i also has statistical error (σ_B). Using the covariance matrix for $\vec{\theta}$, we can estimate σ_B via standard Gaussian error propagation[‡] (see Barlow 1993, for a review of standard Gaussian error propagation). Error propagation assuming that the resulting error distribution is Gaussian leads to Gaussian uncertainties on the model estimated B_i quite naturally[§].

We must use a likelihood for Poisson data with a Gaussian background to fit the spectral data. This is embodied in the PG-statistic (Arnaud et al. 2015):

$$-2 \log L = 2 \sum_{i=1}^N M_i + t_s f_i - S_i \log(M_i t_s f_i) + \frac{1}{2\sigma_{B,i}^2} (B_i - t_s f_i)^2 - S_i (1 - \log S_i). \quad (5)$$

Here, t_s is the source interval duration and f_i is the profiled-out background model[¶]. This is the statistic we will minimize in our spectral analysis.

In the RMFIT software, the background is assumed to be perfect with no variance. Therefore, only the total counts are assumed to have statistical variability. To deal with this, RMFIT modifies the Poisson likelihood by adding the estimated background from Equation 4 to the estimated spectral model counts:

$$-2 \log L = 2 \sum_{i=1}^N (M_i + B_i) - S_i + S_i (\ln(S_i) - \ln(M_i + B_i)). \quad (6)$$

2.3. Method comparison: spectral simulations

Since it is possible that the method of Blackburn et al. (2015) recovers a significant fluctuation above the typical background, it is important to understand if the source has the spectral parameters reported in Connaughton et al. (2016). Therefore, we simulate the problem. We fit the background of the data before the trigger over a duration of 10 s to obtain the average background rate in each channel. We then simulate 10 s background from this sampled spectrum assuming each channel has Poisson fluctuations with their means derived from the sampled spectrum. Next, we simulate a one second source with a power law spectrum. We choose the power law index to be -1.4 and three different amplitudes: $A=2 \cdot 10^{-3}, \cdot 10^{-4}, 0.0$. The first amplitude models the claim of Connaughton et al. (2016), the second simulates an order of magnitude weaker source, and finally the last amplitude implies no source. For each set of spectral parameters, we generate 100 sets of source and background simulations and create TTE data via the method described in Burgess (2014).

For each simulation, we fit the simulated source spectra with three different methods. First, we fit the background and spectrum in RMFIT. Next, we use the Poisson method to fit the background, and fit the source spectra with the standard PGStat statistic. To minimize the likelihood, we use MINUIT and our own RSP matrix convolution software for computational simplicity (hereafter MLEfit), but verified our results by producing PHA files for source and background and fitting them with XSPEC**. We effectively compare three different methods for fitting spectra. Figure 3 shows the results of the simulations where we assume the same source spectrum reported in Connaughton et al. (2016).

MLEfit using PGStat recovers the true simulated amplitude more accurately than any other method. The same has been shown to be true for a simulation of different spectral slopes at identical amplitudes (see Fig. 7.3. in Arnaud et al. 2011). RMFIT is biased to slightly higher amplitude values. When the source amplitude is reduced by an order of magnitude, MLEfit is about to find the correct amplitude with either statistic though the modified C-stat is slightly biased towards higher values. On the other hand, RMFIT recovers a source amplitude resembling what is

[‡] Assuming that the error distribution of the coefficients is Gaussian which should be safe. If they are not then we cannot employ standard error propagation without Monte Carlo methods.

[§] The fact that the estimated background model has a Gaussian error distribution should not be confused with the fact that the background data is Poisson distributed.

[¶] see <https://heasarc.gsfc.nasa.gov/xanadu/xspec/manual/XSappendixStatistics.html> for details.

** Unfortunately, XSPEC does not have the modified C-stat used in RMFIT or we could perform our full analysis with XSPEC.

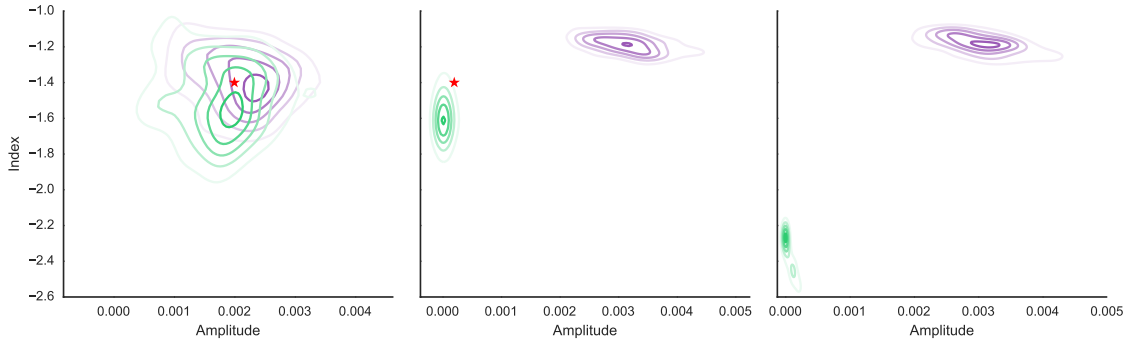


Figure 3. Recovered parameters from simulated spectra of a power law with index -1.4 and assuming the source amplitude is $0.002 \text{ ph cm}^{-2} \text{ s}^{-1}$ (left panel), 0.0002 (middle) or zero (no source; right). The results of RMFIT are shown in purple and our MLEfit in green. The true parameters are indicated with a red star.

found in [Connaughton et al. \(2016\)](#) (see Figure 3). Similarly, when there is no source, MLEfit finds a source amplitude near zero, while RMFIT still finds a source amplitude of $\sim 3 \cdot 10^{-3}$. This has two implications. MLEfit is able to distinguish between source and background while RMFIT is including background in its source spectrum. The fact that RMFIT finds a source spectrum similar to what is reported in [Connaughton et al. \(2016\)](#) even when there is *no source* indicates that the background spectrum can be modeled with a power law having an amplitude and overall spectrum very similar to the reported source spectrum in [Connaughton et al. \(2016\)](#). We further demonstrate this in the following section.

Combining the low count bias of χ^2 which can underestimate the background level and the assumption of no variance on this underestimated background via the use of RMFIT’s modified C-stat, it is possible to find a source spectrum and flux that is unrealistically too large as we will demonstrate using our approach to spectral fitting.

3. ANALYSIS OF THE GBM EVENT

3.1. Results with RMFIT

Following [Connaughton et al. \(2016\)](#), we generate 10 sets of detector response matrices (RSPs) corresponding to the 10 locations listed in the same work, using the standard stand-alone response generator. We use the GBM team created software, RMFIT to bin the data, make energy selections equivalent with those in [Connaughton et al. \(2016\)](#), as well as fit the background to the surrounding count light curve. We fit a power-law spectrum to the data, using the 10 different RSPs discussed above. Table 1 details these fits. Within the statistical errors, these are compatible with the spectra derived by [Connaughton et al. \(2016\)](#), in particular the details given in their sect. 3.2 and Fig. 5.

Table 1. GBM spectral parameters (and their 1σ errors) at 10 positions along the LIGO arc, derived with RMFIT and with PGStat.

RA (deg)	DEC (deg)	RMFIT-based analysis			PGStat-based analysis		
		Amplitude ($\text{ph}/\text{cm}^2/\text{s}$) (@100 keV)	Index	Fluence ($10^{-7} \text{ erg}/\text{cm}^2$) (10–1000 keV)	Amplitude ($\text{ph}/\text{cm}^2/\text{s}$) (@100 keV)	Index	Fluence ($10^{-7} \text{ erg}/\text{cm}^2$) (10–1000 keV)
84.0	-72.8	0.0043 ± 0.0020	-1.44 ± 0.14	4.3 ± 1.5	0.0035 ± 0.0031	-1.85 ± 0.86	2.7 ± 2.6
155.3	-43.2	0.0019 ± 0.0006	-1.26 ± 0.11	2.1 ± 0.6	0.0008 ± 0.0005	-1.50 ± 0.25	0.8 ± 0.5
102.0	-73.9	0.0039 ± 0.0016	-1.42 ± 0.13	3.9 ± 1.2	0.0025 ± 0.0020	-1.93 ± 0.43	1.9 ± 1.6
118.3	-72.9	0.0034 ± 0.0013	-1.39 ± 0.12	3.5 ± 1.0	0.0018 ± 0.0019	-1.79 ± 0.42	1.4 ± 1.3
132.0	-70.4	0.0030 ± 0.0011	-1.36 ± 0.12	3.2 ± 0.9	0.0014 ± 0.0014	-1.72 ± 0.39	1.1 ± 1.0
140.9	-66.6	0.0026 ± 0.0009	-1.33 ± 0.11	2.9 ± 0.8	0.0014 ± 0.0011	-1.69 ± 0.32	1.1 ± 0.9
147.5	-62.5	0.0024 ± 0.0008	-1.31 ± 0.11	2.7 ± 0.7	0.0009 ± 0.0007	-1.57 ± 0.32	0.8 ± 0.6
151.2	-58.0	0.0022 ± 0.0007	-1.29 ± 0.11	2.5 ± 0.7	0.0009 ± 0.0006	-1.54 ± 0.28	0.8 ± 0.6
153.4	-53.1	0.0020 ± 0.0007	-1.28 ± 0.11	2.4 ± 0.6	0.0009 ± 0.0006	-1.50 ± 0.26	0.8 ± 0.6
153.9	-48.2	0.0019 ± 0.0006	-1.27 ± 0.11	2.2 ± 0.6	0.0009 ± 0.0005	-1.49 ± 0.25	0.8 ± 0.5

We note that we have used the full 128-channel TTE data instead of the 8-channel TTE data used in [Connaughton et al. \(2016\)](#), because a proper MLE statistic is accurate regardless of the binning as pointed out in [Cash \(1979\)](#).

3.2. Spectral Variations of the Background

The source spectrum reported in [Connaughton et al. \(2016\)](#) is more similar to the background (cosmic X-ray background plus Earth albedo spectrum; [Ajello et al. 2008](#)) than of short GRBs. In Section 2.3, we demonstrated that RMFIT will effectively find a source spectrum even when no source is present and is therefore fitting strong, positive fluctuations of the background. To further assess this claim, we fit 1.024 second intervals before and after the tentative detection. We iteratively select the intervals as source and fit the surrounding light curve as background. We use the Cash statistic to fit the background and MLEfit with PGStat to fit the source since we have demonstrated that the RMFIT methods are insufficient for low-count analysis. As an additional check, we also fit the spectra with RSPs generated from each of the 10 locations used in [Connaughton et al. \(2016\)](#).

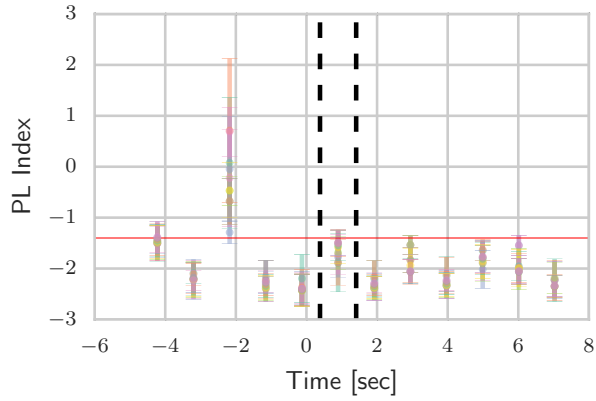


Figure 4. Variation of spectral slopes of power-law spectra fitted to the residual flux after background subtraction. The vertical dashed lines show the interval of the putative event, and the red horizontal line the spectral index for the best-fit position from [Connaughton et al. \(2016\)](#). For each time interval, the power law indices of all 10 positions along the LIGO localisation arc are shown.

Figure 4 shows that the spectra of the surrounding time intervals are very similar to the spectral parameters of the putative event, regardless of position on the sky used to generate the RSPs. Since the location is poorly constrained, then the range of parameters covered by these plots could be considered valid. Therefore, all recovered spectra are essentially the same indicating that the source is most likely a strong positive background fluctuation.

4. SPECTRAL ANALYSIS WITH PROPER STATISTICS

4.1. Spectral analysis with Cash and PGStat

Here, we demonstrate the spectrum of the source candidate using Cash statistics to fit the background, and PGStat to fit the spectra. Table 1 shows the best fit for each of the 10 locations across the LIGO localisation arc. As can be seen, the amplitudes are much lower and the fluences reduced correspondingly. Also, the spectral slope is substantially softer. It is still most likely that the source is a strong background fluctuation, because the spectrum is not inconsistent with zero, and consistent with what is expected from the combination of extragalactic background and Earth’s albedo. While the larger error in spectral slope still allows a hard spectrum, the reality of these solutions is excluded by the INTEGRAL/ACS limits (see end of this section, and the next one).

Next, we examine the predicted counts from our spectral fits with MLEfit, RMFIT, and those reported in [Connaughton et al. \(2016\)](#). Figure 5 shows the count light curve of NaI 5 integrated over 11.5–930 keV. The background model coming from the polynomial fit is shown with its 1σ Gaussian errors. The total Poisson error of the event is not too far from the background, and indeed there are several peaks of similar amplitude within this time slice. Using the RSP corresponding to RA = 155.3, Dec = -43.2 and the spectral parameters corresponding to the fits at that location (see e.g. row 2 of Table 1), we convolve the power-law photon model to produce the predicted number of counts during the event. The counts predicted from MLEfit are within the observed range of background subtracted counts, but the results from our own RMFIT fits and those of [Connaughton et al. \(2016\)](#) (using RMFIT) over-predict the number of counts significantly.

4.2. Bayesian approach

As a secondary check, we attempt a Bayesian fit of the data where both the background polynomials in each channel and the spectra are fit simultaneously. This avoids the ambiguity of background error propagation and allows us to directly assess the background’s effect on the spectral fit. The method will be detailed in [Burgess \(2016, in prep.\)](#),

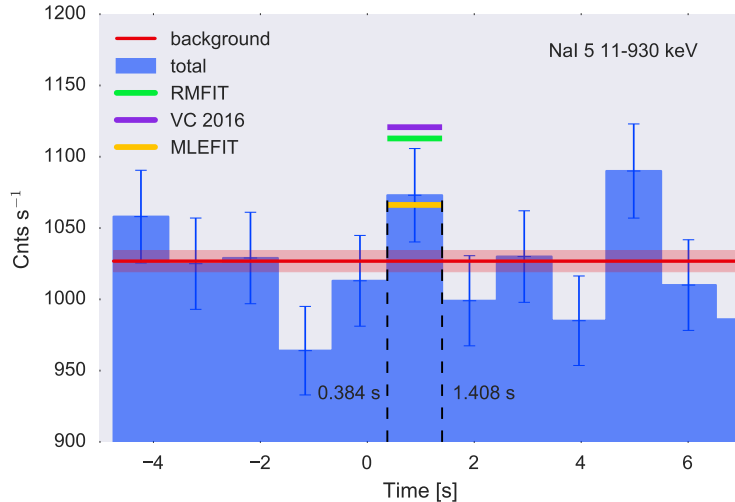


Figure 5. The total, raw count light curve of NaI 5 (blue) integrated over 11–930 keV. The modeled background (red) with shaded 1σ Gaussian error is shown in red. Using the GBM DRM, we calculate the predicted counts from power law fits using our method (yellow), our fit with RMFIT (green) and the parameters reported in [Connaughton et al. \(2016\)](#). Both methods that rely on RMFIT over-predict the expected counts. Additionally, it is easy to see that there are spikes in the raw light curve that are equally as bright as the alleged event.

however, we briefly detail the approach here. The full temporal and spectral model is defined as a piecewise function in time:

$$f(t^i, \varepsilon; \theta_n^j, \vec{\phi}) = \begin{cases} B(t^i; \theta_n^j) & t^j < t_{\text{start}} \\ B(t^i; \theta_n^j) + S(t^i, \varepsilon; \vec{\phi}) & t_{\text{start}} \leq t^j \leq t_{\text{stop}} \\ B(t^i; \theta_n^j) & t^j > t_{\text{stop}} \end{cases}$$

where t^i is the time in the i^{th} interval, θ_n^j is the j^{th} -order polynomial coefficient in the n^{th} energy channel, B is the background polynomial, and S is the source photon model with $\vec{\phi}$ parameters. The t_{start} and t_{stop} correspond to the source interval times. For the data at hand, we use a zero-order polynomial, B in each channel and again choose a power-law function for S . A log-uniform prior is chosen for θ_n^0 and the power law amplitude and a uniform prior for the power law spectral index. Unlike the previous analysis, we are fitting both the background and source simultaneously, so we can take both the background and source as distributed via the Poisson process.

Figure 6 shows the resulting parameter posterior contours indicating that the parameters are mostly unconstrained and the amplitude is not inconsistent with zero. Moreover, Figure 7 shows the light curves from the data with the background and source + background posteriors for the NaI and BGO detectors. The source + background histogram is clearly consistent with the background only, suggesting that the source is a background fluctuation and not an astrophysical source.

We again simulate the spectral parameters in [Connaughton et al. \(2016\)](#) to test if this method could recover the parameters of a real source. Figures 8 and 9 show the results indicating that a true source with the reported spectral parameters would be recovered by the method.

To access the presence of an actual source, we use the Bayesian tool to fit the data using the background polynomial only. Using the Monte Carlo samples from the source + background fit and the background only fit, we compute the deviance information criteria (DIC) ([Spiegelhalter et al. 2002](#)) for each model which allows us to perform model comparison between them. The DIC compares model fit and penalizes for model complexity which can be a function of both data and model. We find a DIC of 18341 and 18347 for background only and source+background respectively. Choosing the lowest DIC implies that the background only model is the best description of the data. This proposes an interesting contrast to the claimed detection in [Connaughton et al. \(2016\)](#) via the method of [Blackburn et al. \(2015\)](#). It is likely that the included information in the simultaneous fit of the full resolution data is a better characterization and this method correctly finds no significant source in agreement with theory and the non-detection in all other observatories.

4.3. Re-analysis of short GRBs

Based on the previous analysis, we conjecture that the mismatch in the resulting parameters depends on the statistical significance of the residual source counts per event. In order to test this conjecture, we re-analyzed with PGStat all 58 short GRBs from the GBM time-integrated 4-yr catalog ([Gruber et al. 2012](#)), which had the powerlaw model as

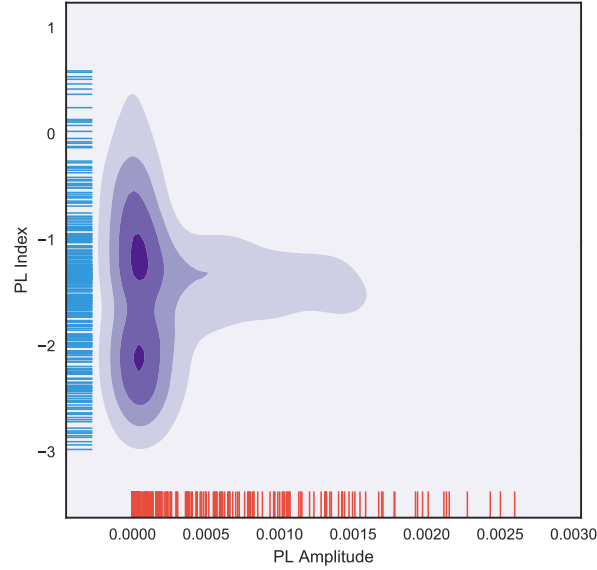


Figure 6. The posterior contours of the power law fit to the event. The blue and red rug plots indicate the distributions of the power law index and amplitude, respectively. The parameters are poorly constrained and not inconsistent with zero amplitude.

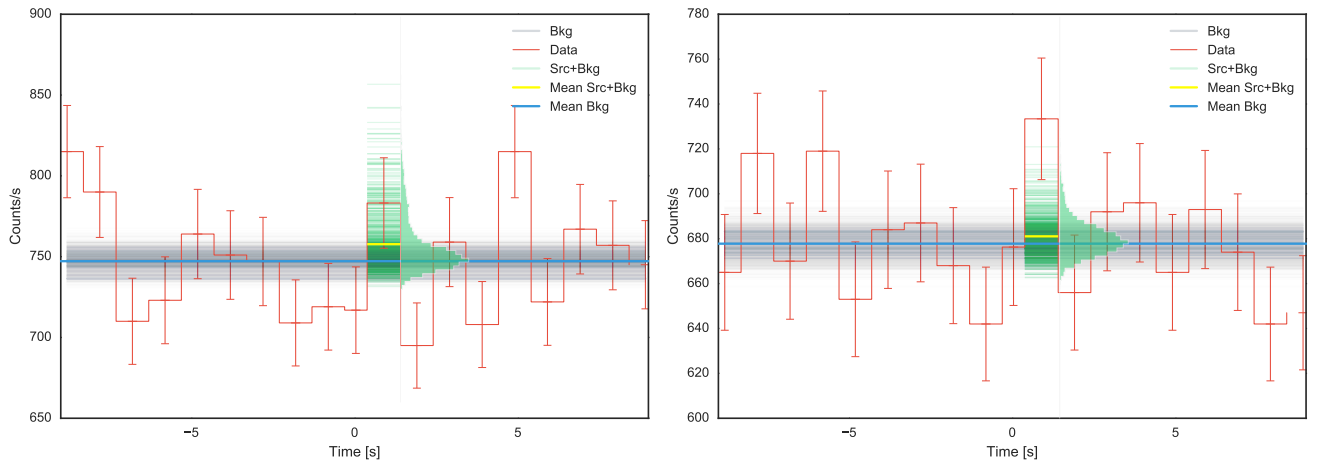


Figure 7. The data from the NaI (left) and BGO (right) superimposed with the background and source+background posteriors. The source+background posterior (green histogram) clearly shows that the source is consistent with zero, i.e., background.

BEST-fit model. Fig. 11 shows the comparison of the resulting parameters with those obtained using RMFIT (and listed in Gruber et al. 2012). We find that PGStat reproduces the fit parameters of RMFIT for strong GRBs, while for faint GRBs the spectra are systematically softer and the fluences smaller, exactly as shown in the above analysis of the GBM event.

The above analysis demonstrates the systematic effect of the differences between the RMFIT package and the PGStat analysis. We can go one step further and ask, how the different best-fit parameters affect the prediction of the detectability by INTEGRAL/ACS, and how these predictions compare with the actual detections by INTEGRAL/ACS? Taking two short GRBs from the (Gruber et al. 2012) catalog which belong to the 20% lowest fluence group, we fold the spectral parameters (with their catalog sky position) through the INTEGRAL/ACS response and obtain predictions in the $3-4\sigma$ range. Checking the INTEGRAL/ACS, we indeed find these GRBs at these confidence levels, demonstrating that our PGStat analysis provides results which are verified by detections with an independent instrument. These two short GRBs are added in Figures 11 and 12. As previously, RMFIT overpredicts the counts, and correspondingly the fluence in INTEGRAL/ACS.

Typical short GRBs have a spectral index of -1.4 ± 0.2 (Gruber et al. 2012), and our PGStat analysis of the faintest triggered short GRBs finds them at indices as soft as -1.6 (with large errors, see Fig. 12). The best-fit spectral index of the GBM event close to GW150914 GRB 120212353 is -1.6 (for a position outside the LIGO arc), and the spectral

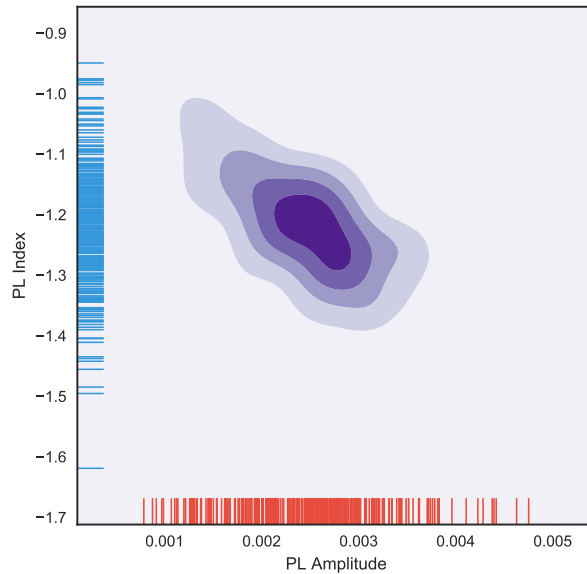


Figure 8. The same as Figure 6 but with simulated data with Amplitude= $0.002 \text{ photons s}^{-1} \text{ cm}^{-2}$ and spectral index = -1.4 . The parameters are well recovered at their simulated values.

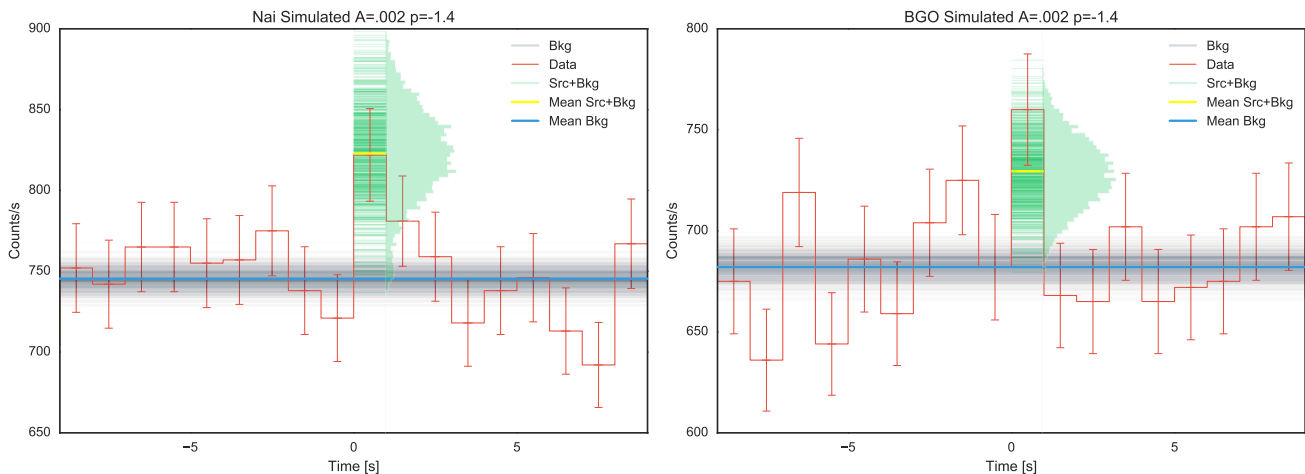


Figure 9. The same as figure 7 but for simulated data. The source+background posteriors (green histograms) clearly show that the source is not consistent with background as expected.

indices for positions along the LIGO arc cover the range $-2.0 \dots -1.5$ (also with large errors, see Fig. 12). While there is some overlap between the two distributions, the GBM-GW150914 event is systematically softer than even the softest/faintest short GRBs.

We can take it yet another step further and test the validity of the PGStat analysis using GBM sub-threshold short GRBs, i.e. GRBs which were detected by Swift/BAT, but not by GBM. We pick two GRBs (one faint and one stronger) out of the 7 for which Burns et al. (2016) determined visibility by GBM, and which were recovered in ground-based searches of the untriggered GBM data (see Table 4 of Burns et al. 2016). For these bursts, the PGStat analysis results in slightly softer and dimmer spectra than the analysis with RMFIT, consistent with the above analysis. The uncertainties in the fluence are small, and exclude zero fluence, i.e. the result recovers proper flux from these two GRBs. This shows that the PGStat analysis is capable of recovering real GBM sub-threshold events. In contrast, PGStat analysis of GW150914-GBM indicates an amplitude consistent with zero.

To further validate the Bayesian method, we apply it to one of these weaker GRBs (GRB 140516A). The method is able to clearly distinguish between source and background (Fig. 10) with a DIC preferring a source even though the total count rate above background is relatively low (even lower than the GBM-GW150914!). This further strengthens our claim that were GBM-GW150914 a real astrophysical short GRB, the method would be able to identify it. Caution must be taken when assessing the presence of a source based on total count rate alone when spectral information is

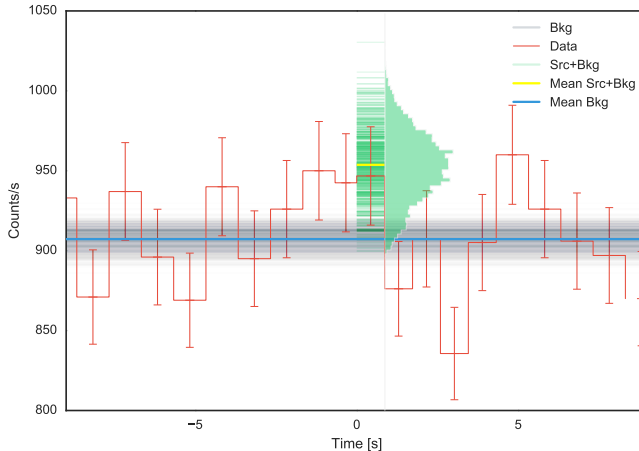


Figure 10. The count rate from GRB 140516A in NaI 01 super-imposed with the source+background and background posteriors. The DIC between the two models favors source + background, despite the fact that in the broad-band lightcurve the GRB is hardly evident.

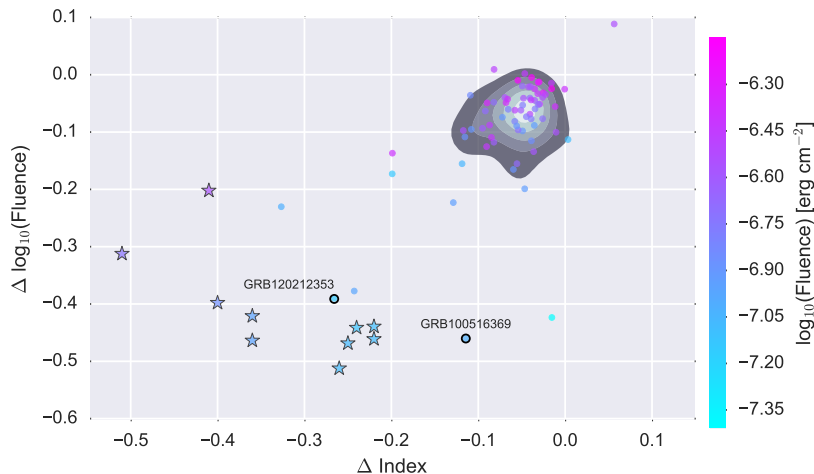


Figure 11. The differences in spectral slope and fluence between analyses using either RMFIT or PGStat, color-coded according to the significance of the residual source counts, and using all short-duration GRBs from Gruber et al. (2012). For bright (short) GRBs the differences in the two approaches are minimal, and within the 1σ errors of the parameter estimates. However, the fainter the bursts, the larger are the changes towards fainter flux and softer spectral slope. The shaded contours contain the $\approx 80\%$ brightest short GRBs (each dot represents one GRB). For two of the faintest short GRBs (encircled and labeled dots), a preliminary consistency check of the PGStat-based parameters with the expected significance in INTEGRAL/ACS finds perfect matches. A more thorough cross-check is presently being performed as a combined effort of the Fermi/GBM and INTEGRAL/ACS teams which will be published separately. The filled stars represent our PGStat-based parameters for the GBM event at the 10 locations along the LIGO arc.

available. The additional spectral information, as well as the variability of the background, place severe constraints on the presence of weak events.

5. INTEGRAL DETECTABILITY

Using the best-fit power law models as derived within RMFIT (Tab. 1), we compute the fluence over the detection range of 50 keV to 4.7 MeV (as Fig. 5 in Connaughton et al. 2016 and consistent with their sect. 3.2).

We then use these position-dependent spectral parameters to simulate the response of ACS for each of these 10 positions, and find that the GBM event should have been detected at $>8\sigma$ everywhere (see Tab. 2). The last column gives the range of significances when accounting for both, the error in spectral slope as well as in amplitude: the smallest significance is still larger than $>5.9\sigma$.

In contrast, if we use the spectral parameters of our own spectral analysis using PGStat, the lower fluences (Tab. 1) result in predictions of typically $<3\sigma$ significance (Fig. 12), consistent with the non-detection of the GBM event with INTEGRAL-SPI/ACS (Savchenko et al. 2016).

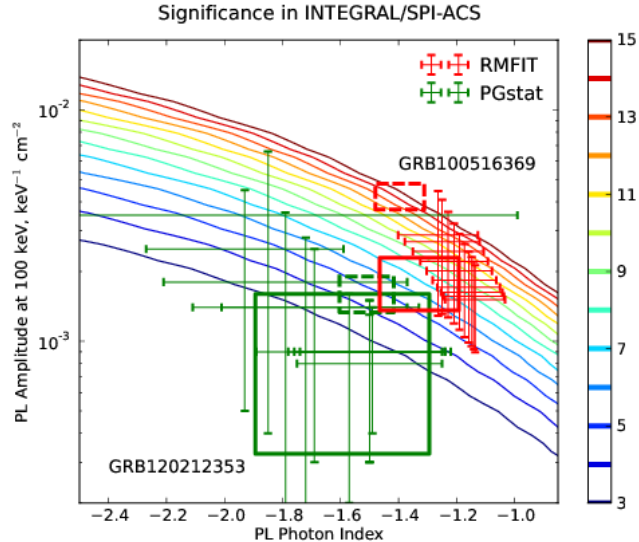


Figure 12. INTEGRAL/SPI-ACS significance map for power law spectra of different slopes from the best-fit position on the LIGO arc as given in [Connaughton et al. \(2016\)](#). With the fluences for a 1 sec transient as given in Tabs. 1 and 2, the green and red crosses show the predicted significances of detection for the claimed GBM event. The rectangles are the faint short GRBs used for verification of the PGStat parameters, and are detected with INTEGRAL/ACS (we note that the significance contours are only approximate for the two real GRBs, and different for each, due to different incidence angle/response and duration).

6. CONCLUSIONS

The event seen by GBM at 0.4 s after the gravitational wave GW150914 is a very faint, sub-threshold event ([Connaughton et al. 2016](#)), not found by any of the standard undirected algorithms designed to pick up untriggered events. Both, the signal-to-noise ratio as well as the false alarm rate reported in [Connaughton et al. \(2016\)](#) depend on the assumed hard spectral shape – a softer spectral shape increases the probability of a background fluctuation.

Based on this and our analysis we conclude that the event ([Connaughton et al. 2016](#)) seen in GBM 0.4 sec after the gravitational wave event GW 150914 ([Abbott et al. 2016](#)) is very likely not an astrophysical event due to three reasons: (i) the spectrum is soft, and softer than typical short-hard GRBs, (ii) the spectrum is consistent with the background spectrum as measured by GBM, (iii) due to our more thorough background treatment, the fluence of the event is substantially fainter, consistent with zero. Combined with the softer slope our spectral deconvolution predicts that INTEGRAL-SPI/ACS should not detect this event, consistent with reality ([Savchenko et al. 2016](#)).

Our conclusion is more consistent with the expectation of no γ -ray emission from binary black hole mergers ([Lyutikov 2016](#)), and requires no effort in significant fine-tuning of models to explain the alleged delay of the gamma-ray emission relative to the gravitational wave emission.

We have further identified issues with the standard GBM fitting tool, RMFIT, in the low-count regime and advocate

Table 2. ACS response to GBM event along the LIGO arc, based on the spectra as deduced with RMFIT, shown in Tab. 1.

RA / Decl. (2000.0)	Fluence (50–4700 keV) (erg/cm ²)	Significance of best-fit (sigma)	Significance range (sigma)
84.0 -72.8	5.71×10^{-7}	12.1	8.1 -18.1
155.3 -43.2	5.39×10^{-7}	8.0	5.9 -10.9
102.0 -73.9	4.96×10^{-7}	11.7	7.9 -17.0
118.3 -72.9	4.58×10^{-7}	10.9	7.6 -15.7
132.0 -70.4	4.26×10^{-7}	10.3	7.2 -14.5
140.9 -66.6	3.98×10^{-7}	9.7	6.9 -13.5
147.5 -62.5	3.79×10^{-7}	9.1	6.6 -12.6
151.2 -58.0	3.66×10^{-7}	8.7	6.3 -12.0
153.4 -53.1	3.55×10^{-7}	8.5	6.1 -11.6
153.9 -48.2	3.46×10^{-7}	8.2	6.0 -11.2

for careful study of the statistics when handling the spectra of marginal detections. We emphasize that RMFIT can be safely used for events in the high-count regime, as has been done in many previous Fermi/GBM publications. In the low-count regime, the PGStat statistics or our Bayesian method properly model the statistical properties of GBM data, and our simulations show that in this case, our results are more accurate than the statistical tools in RMFIT. This has been verified by (i) comparing predictions for INTEGRAL/ACS detectability against its actual performance for short GRBs, as well as (ii) by recognizing faint short GRBs detected by GBM (and confirmed by INTEGRAL/ACS detections) with even smaller significance in the broad-band GBM light curve as the GBM-GW150914 event. Thus, if GBM-GW150914 were a real astrophysical short GRB, our methods would have identified it.

The authors acknowledge V. Connaughton for implementing modifications upon our criticism. We are grateful to B. Anderson and J. Conrad (Stockholm University) for sharing their statistics expertise with us. JG also thanks K. Arnaud for details on the Castor statistics description in the XSPEC manual. This research made use of PyMC3 a probabilistic programming language for Bayesian inference (Salvatier et al. 2016), Astropy, a community developed core Python package for Astronomy (Astropy Collaboration et al. 2013), Matplotlib, an open source Python graphics environment (Hunter 2007) and Seaborn (Waskom et al. 2015) for plotting.

The Fermi/GBM project is supported by NASA. Support for the German contribution to GBM was provided by the Bundesministerium für Bildung und Forschung (BMBF) via the Deutsches Zentrum für Luft- und Raumfahrt (DLR) under contract number 50 QV 0301. This research was supported by the DFG cluster of excellence 'Origin and Structure of the Universe' (www.universe-cluster.de).

REFERENCES

- Abbott, B. P., Abbott, R., Abbott, T. D. et al. 2016a, PRL 116, 061102
- Abbott, B. P., Abbott, R., Abbott, T. D. et al. 2016b, ApJ (subm., <https://arxiv.org/abs/1602.08492>)
- Abramowitz, M., Stegun, I.A., 2002, Handbook of Mathematical Functions (<http://www.math.hkbu.edu.hk/support/aands/index.htm>)
- Ajello, M., Greiner, J., Sato, G. et al. 2008, ApJ 689, 666
- Andrae, R., Schulze-Hartung, T., Melchior, P. et al. 2010, arXiv:1012.3754
- Arnaud, K., Smith, R., Siemiginowska, A., 2011, Handbook of X-ray Astronomy, Cambridge Univ. Press
- Arnaud, K., Dorman, B., Gordon, C. 2015, Xspec User's Guide v12.9.0, <https://heasarc.gsfc.nasa.gov/xanadu/xspec/manual/XSappendixStatistics.html>
- Astropy Collaboration et al., 2013, A&A 558, A33
- Baker, S., Cousins, R. D., 1984, NIM 221, 437
- Barlow, R. 1993, Statistics: A Guide to the Use of Statistical Methods in the Physical Sciences
- Belczynski K., Dominik M., Bulik T. et al. 2010, ApJ 715, L138
- Blackburn, L., Briggs, M. S., Camp, J. et al. 2015, ApJS 217, 8
- Burgess, J. M. 2014, MNRAS 445, 2589
- Burgess, J. M. 2016 (in prep.)
- Burns, E., Connaughton, V., Zhang, B.-B., et al. 2016, ApJ 818, 110
- Cash, W. 1979, ApJ 228, 939
- Connaughton, V., Burns, E., Goldstein, A. et al. 2016, ApJ (arXiv:1602.03920.v3)
- Gruber, D., Goldstein, A., Weller von Ahlefeld, V. et al. 2012, ApJS 211, 12
- Humphrey, P.J., Liu, W., Buote, D.A., 2009, ApJ 693, 822
- Hunter, J.D., 2007, Computing In Science & Engineering 9, 90
- Lyutikov, M. 2016, (subm.; arXiv:1602.07352)
- Perna R., Lazzati D., Giacomazzo B., 2016, ApJ 821, L18
- Salvatier J., Wiecki T.V., Fonnesbeck C., 2016, Probabilistic programming in Python using PyMC3. PeerJ Computer Science 2:e55, <https://doi.org/10.7717/peerj-cs.55>
- Savchenko, V., Ferrigno, C., Mereghetti, S. et al. 2016, ApJ 820, L36
- Scargle, J.D., Norris, J.P., Jackson, B., Chiang, J. 2013, ApJ 764, 167
- Skellam, J.G., 1946, Journal of the Royal Stat. Soc., Ser. A, 109, 296
- Spiegelhalter D.J., Best N.G., Carlin B.P., van der Linde A., 2002, J. Royal Statist. Soc., Ser. B, 64 (4)
- Waskom M., Botvinnik O., Hobson P. et al. 2016, <http://dx.doi.org/10.5281/zenodo.45133>
- Wilks, S.S, 1938, The Annals of Mathematical Statistics 9 (1)